Russian Journal of Earth Sciences Online ISSN: 1681-1208

Variability of the Dome-Like Form of the Deep Water Temperature in the Weddell Sea Based on ORAS5 Reanalysis

V. V. Bagatinskaya[1,2,*], V. A. Bagatinsky[1,2,3], E. G. Morozov[3,*], N. A. Diansky[1,2,4], and A. V. Gusev[2,3,4]

[1]Lomonosov Moscow State University, Faculty of Physics, Moscow, Russian Federation
[2]Zubov State Oceanographic Institute, Moscow, Russian Federation
[3]Shirshov Institute of Oceanology of Russian Academy of Sciences, Moscow, Russian Federation
[4]Marchuk Institute of Numerical Mathematics of Russian Academy of Sciences, Moscow, Russian Federation
* **Correspondence to:** Varvara Bagatinskaya, bagatinskayavv@my.msu.ru, Evgeny Morozov, egmorozov@mail.ru

Abstract: The variability of the dome-like form position of the Weddell Sea Deep Water (WSDW) has been studied based on ORAS5 datasets. According to these data, the upper boundary of the deep water occupied the highest position during most of 2005, and the lowest position in 2014 relative to its mean for 1993–2023. This change occurred because of the intensification of negative wind vorticity in 2005 and its weakening in 2014. Between 1993 and 2023, a permanent water transport from the Weddell Sea to the Scotia Sea was detected over the depth corresponding to the sill in the Orkney Passage in the ORAS5 data. In 2005, this transport was almost unchanged, whereas in 2014 it became stronger. When the dome boundary of WSDW moves up in the central part of the Weddell Sea, the outer parts of the dome move down, and vice versa. In the northern part of the Weddell Sea, this motion of isotherms and isopycnals causes either colder or warmer water parts of the WSDW column to overflow the crest of the South Scotia Ridge and continue its motion in the Scotia Sea.

Keywords: Weddell Sea Deep Water, abyssal water, seasonal variability, ORAS5

Citation: Bagatinskaya V. V., Bagatinsky V. A., Morozov E. G., Diansky N. A., and Gusev A. V. (2026), Variability of the Dome-Like Form of the Deep Water Temperature in the Weddell Sea Based on ORAS5 Reanalysis, *Russian Journal of Earth Sciences*, 26, ES1014, EDN: RJQAVW, https://doi.org/10.2205/2026es001088

1. Introduction

The north-directed transport of Antarctic Bottom Water (AABW) from the Weddell Sea to the Scotia Sea occurs through a few conduits over the crest of the South Scotia Ridge. It was estimated in [*Naveira Garabato et al.*, 2002] that the transport of Weddell Sea Deep Water (WSDW) from the Weddell Sea through the South Scotia Ridge is 6.7±1.7 Sv. The Orkney Passage (based on the echo sounder data, the depth of the transversal sill is 3600 m) is the main conduit of bottom water from the Weddell Sea to the north. After overflowing, the potential temperature of the outflowing water is slightly below −0.50 °C [*Morozov et al.*, 2022] (Figure 1).

The intensity of AABW outflow from the Weddell Sea varies in time on the interannual and seasonal time scales. The colder transport of bottom waters occurs in May/June, while the warmer does in October/November. In addition, the transport varies from one year to another [*Gordon et al.*, 2010]. The years 1999 and 2002 were characterized by the coldest water transport for the time series of observations. On the contrary, no cold phase has been detected [*Gordon et al.*, 2010] in 2000. It was found that the origin of pulses in colder and warmer waters is in the southwestern Weddell Sea. Interannual variations are related to the cyclonic wind structure over the Weddell Sea caused by large-scale climatic processes. Winds over the Weddell Sea drive the seasonal cycle in the transport and properties of WSDW.

Observations in the Scotia Sea and analysis reported in [*Abrahamsen et al.*, 2019] revealed that, since 2014, the decrease in the transport of AABW stopped. This decrease in the WSDW transport has been observed since 1990s. After 2014, the WSDW transport became stable and even partly increased.

Research Article

Received: September 29, 2025
Accepted: November 19, 2025
Published: April 9, 2026

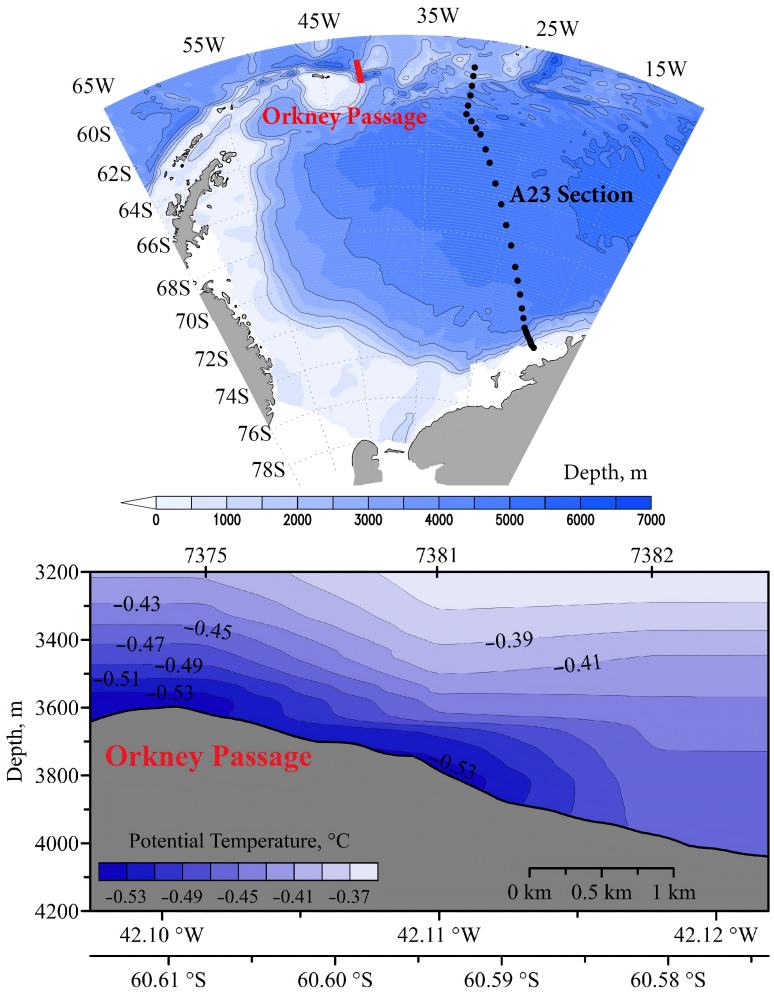

Figure 1. (top) Locations of stations along section A23 in the Weddell Sea in 1995 (black dots): expedition onboard the vessel "James Clark Ross", cruise 10, March–April 1995, the red bar marks the section in the Orkney Passage; (bottom) Cold water overflowing the Orkney Passage (the red bar on the top panel) [*Morozov et al.*, 2022]: black lines are potential temperature contours.

Fluctuations in the potential temperature of AABW in the Vema Channel that we have been observing since 1972 [*Campos et al.*, 2021] and temperature variations in the Argentine Basin are caused by varying temperatures of the AABW transported through the Orkney Passage to the Scotia Sea [*Morozov et al.*, 2021]. We support the interpretation of variations in this flux from the Weddell Sea suggested in [*Coles et al.*, 1996; *Meredith et al.*, 2008]. The export of WSDW from the Weddell Sea is governed by atmospheric forcing. Intensity of the cyclonic gyre in the Weddell Sea influenced by the forcing changes the slope of isopycnal surfaces, which are either flattened or steepened. This influences the density and potential temperature of WSDW propagating through the Orkney Passage to the Scotia Sea. In the context of this paper, we refer to WSDW as the water in the dome-shaped layer with potential temperatures in the range $-0.7 < \theta < 0.2\,^{\circ}\mathrm{C}$ occupying a region within 60–67°S and 10–25°W. The depth of the ridge crest in the Orkney Passage is 3600 m, which is close to the depth of the isotherm $-0.6\,^{\circ}\mathrm{C}$. After passing the Orkney Passage, the temperature of WSDW becomes greater than $-0.54\,^{\circ}\mathrm{C}$ (Figure 1).

For the strong wind periods the cyclonic gyre in the Weddell Sea intensifies, the outer parts of isopycnals and isotherms deepen, and lighter water overflows the sill. Thus, warmer water is transported northward. For the weak wind periods, the upper boundary of WSDW becomes shallower, and colder water flows northward into the Scotia Sea. After the large volumes of bottom water move through the Scotia Sea, they circulate in the Argentine Basin.

Figure 2 shows the distribution of potential temperature over a section in the Orkney Passage based on the measurements over the World Ocean Circulation Experiment (WOCE) section A23 (left panel). The right panel shows two types of isopycnals: under weak wind forcing (dashed lines) and strong one leading to the stronger rotation in the Weddell Gyre (solid lines).

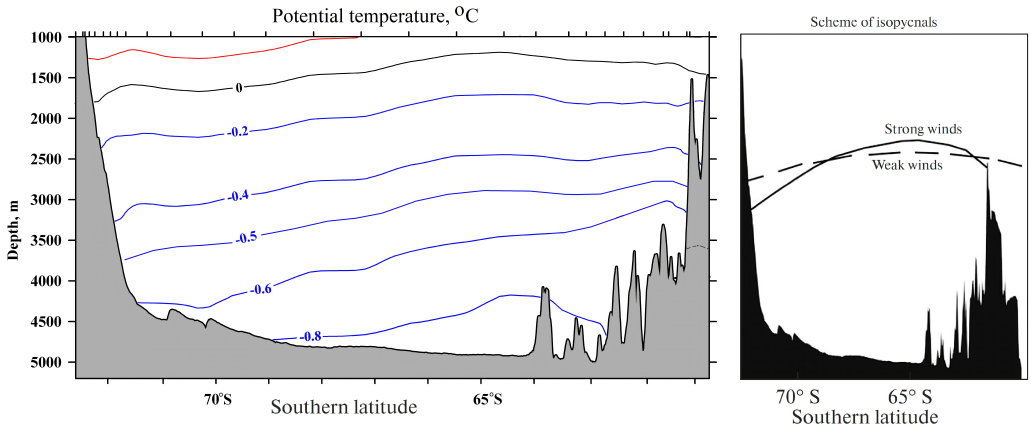

Figure 2. (left) Potential temperature (°C) section in the Weddell Sea based on the measurements over WOCE section A23 in (black dots in Figure 1) the Weddell Sea in March and April 1995. (right) Scheme of isopycnals in the Weddell Sea during the periods of strong and weak winds. Ticks at the top axis indicate CTD-casts.

One of the mechanisms for maintaining the dome is deep convection in the gyre maintained by the influx of salter and warmer water from the Antarctic Circumpolar Current (ACC) [*Gouretski and Danilov*, 1993] and strong cooling at the gyre surface.

The article studies the role of the cyclonic wind intensity over the Weddell Sea in interannual variations of the bottom water dome and WSDW overflow into the Scotia Sea. It has been confirmed first by experiments with the ocean circulation model that cyclonic wind over the Weddell Sea maintains a dome-shaped structure of water masses represented with isopycnals and isotherms. When the wind weakens, the circulation slows down, the dome moves down, and the WSDW transport increases, and when wind strengthens, the circulation spins up, the dome moves up, and the WSDW transport decreases.

The detailed scheme illustrating general spatial extent of main water masses (e.g., AABW, WSDW), typical directions of their transport (Orkney Passage), their connection with bathymetry of the Weddell Sea, as well as locations of the mentioned areas are presented in [*Morozov et al.*, 2024] in figures 1–3, 5 and 12.

2. Materials and Methods

In the scope of the study, we analyze Ocean ReAnalysis System 5 (ORAS5) datasets covering the period 1993–2023. The data description is presented in Table 1. The data were obtained by European Centre for Medium-Range Weather Forecasts (ECMWF) by using the models Nucleus for European Modeling of the Ocean (NEMO) [*Keeley et al.*, 2024] and Louvain-la-Neuve sea Ice Model (LIM) [*Keeley and Mogensen*, 2018] based on the data EN4 (Version 4 of EN datasets from ENACT/ENSEMBLES) [*Gouretski and Reseghetti*, 2010].

Ocean and sea ice reanalyses (ORAs, or ocean syntheses) are reconstructions of the ocean and sea ice states using an ocean–sea-ice coupled model driven by atmospheric surface forcing and constrained by ocean observations via a data assimilation method [*Balmaseda et al.*, 2015]. The NEMO ocean model version 3.4.1 [*Madec and the NEMO team*, 2008] was used for ORAS5 in the global configuration ORCA025.L75 [*Bernard et al.*, 2006] with the tripolar grid, which allows one to resolve eddies approximately between 50°S and 50°N [*Penduff et al.*, 2010]. The model horizontal resolution is approximately 25 km in the tropics with refinement up to 9 km in the Arctic. There are 75 vertical levels with spacing increasing from 1 m at the surface to 200 m in the deep ocean. The NEMO is coupled to

Table 1. Description of ORAS5 datasets [*Zuo et al.*, 2019].

Data type	Gridded
Projection	Tripolar model grid
Horizontal coverage	Global
Horizontal resolution	~0.25° × 0.25° (~ 25 km in the tropics and 9 km in the Arctic)
Vertical coverage	Depends on the variable: Single level: two-dimensional variables (2D) All levels: three-dimensional variables (3D) from 0 m (sea level) to approximately 5500 m depth
Vertical resolution	Depends on the variable: Single level: 2D variables All levels: 75 ocean model levels for 3D variables
Temporal coverage	From January 1958 to present without gaps Consolidated product: 1958 to 2014 Operational product: 2015 to present
Temporal resolution	Monthly
Ensemble	Five members with perturbations in initial conditions, forcings and observations
Spin-up	Spin-up with five ensemble members and different parameter choices
Grids model	~0.25°, 75 vertical levels NEMO 3.4, LIM2 sea ice model, wave effects TKE mixing in partial ice cover updated wave effects
Forcing	ERA40 (before 1979) ERA-Interim (1979–2015) ECMWF NWP (2015–present) bulk formula + wave forcing
Assimilation	3D-Var FGAT with 5-d window Observation quality control Mean dynamic topography for altimeter data assimilation
Bias correction	Adaptive bias correction scheme ensemble-based bias estimation stability check
SST	HadISST2 + OSTIA operational [*Donlon et al.*, 2012]
	Observations for assimilation
T/S profile	EN4 with XBT and MBT correction [*Gouretski and Reseghetti*, 2010] + NRT
SLA	AVISO DT2014 [*Pujol et al.*, 2016] + NRT
Sea ice	ERA40 + Reynolds OIv2d [*Reynolds et al.*, 2007] + OSTIA reprocessed + OSTIA operational

Note: 3D-Var – 3-Dimensional Variational data assimilation; AVISO – Archiving, Validation and Interpretation of Satellite Oceanographic data; DT – Delayed Time; ECMWF – European Centre for Medium-Range Weather Forecasts; EN4 – Version 4 of EN datasets (ENACT/ENSEMBLES); ERA – ECMWF ReAnalysis; FGAT – First Guess at Appropriate Time; HadISST – Hadley Center Sea Ice and Sea Surface Temperature data set; MBT – Mechanical Bathythermograph; NRT – Near Real-Time; NWP – Numerical Weather Prediction; OIv2d – Optimal interpolation, 2-Dimensional version; ORAS5 – Ocean ReAnalysis System 5; OSTIA – Operational Sea Surface Temperature and Ice Analysis; SLA – Sea Level Anomaly; SST – Sea Surface Temperature; TKE – Turbulent Kinetic Energy; XBT – eXpendable Bathythermograph.

the Louvain-la-Neuve sea ice model version 2 (LIM2, see [*Fichefet and Maqueda*, 1997]) implemented with the viscous-plastic (VP) rheology. The wave effects [*Breivik et al.*, 2015] were implemented in ORAS5 with updated ocean mixing terms for wind. Given that the wave field is not defined under sea ice, the wave impact in the turbulent kinetic energy (TKE) scheme is not used in this case. Instead, a constant value 20 is used under sea ice as a coefficient of the surface input of TKE in ORAS5 [coeff. α_{CB} in eq. (17) in *Breivik et al.*, 2015]. The detailed ORAS5 description is presented in [*Zuo et al.*, 2019].

The analysis of near-surface variability of wind vorticity was performed by using the datasets ERA5 (https://www.ecmwf.int/en/forecasts/dataset/ecmwf-reanalysis-v5). ERA5 is the fifth generation ECMWF atmospheric reanalysis of the global climate covering the period from January 1940 to present. ERA5 is produced by the Copernicus Climate

Change Service (C3S) at ECMWF. ERA5 provides hourly estimates of a large number of atmospheric, land and oceanic climate variables. The data cover the Earth on a 31 km grid and resolve the atmosphere using 137 levels from the surface up to a height of 80 km. ERA5 includes information about uncertainties for all variables at reduced spatial and temporal resolutions. ERA5 combines vast amounts of historical observations into global estimates using advanced modeling and data assimilation systems. It is worth noting that ERA5 replaces the ERA-Interim reanalysis which stopped being produced on 31 August 2019. For the analyzed intervals, ERA5 and ERA-Interim are practically indistinguishable, therefore, ERA5 data was used for the analysis.

The potential at 2000 m depth temperature and density was estimated from potential temperature and salinity of ORAS5 dataset with the Thermodynamic Equation of Seawater (TEOS10) [*McDougall and Barker*, 2011].

3. Results

According to ORAS5 datasets, the upper boundary of the central WSDW achieved its maximum rise in 2005 (Figure 3c) and maximum descent in 2014 (Figure 3d). These changes are well pronounced via wind vorticity. In 2005, amplification is observed of the negative wind vorticity over the central Weddell Sea (Figure 3a), while it weakened in 2014 (Figure 3b).

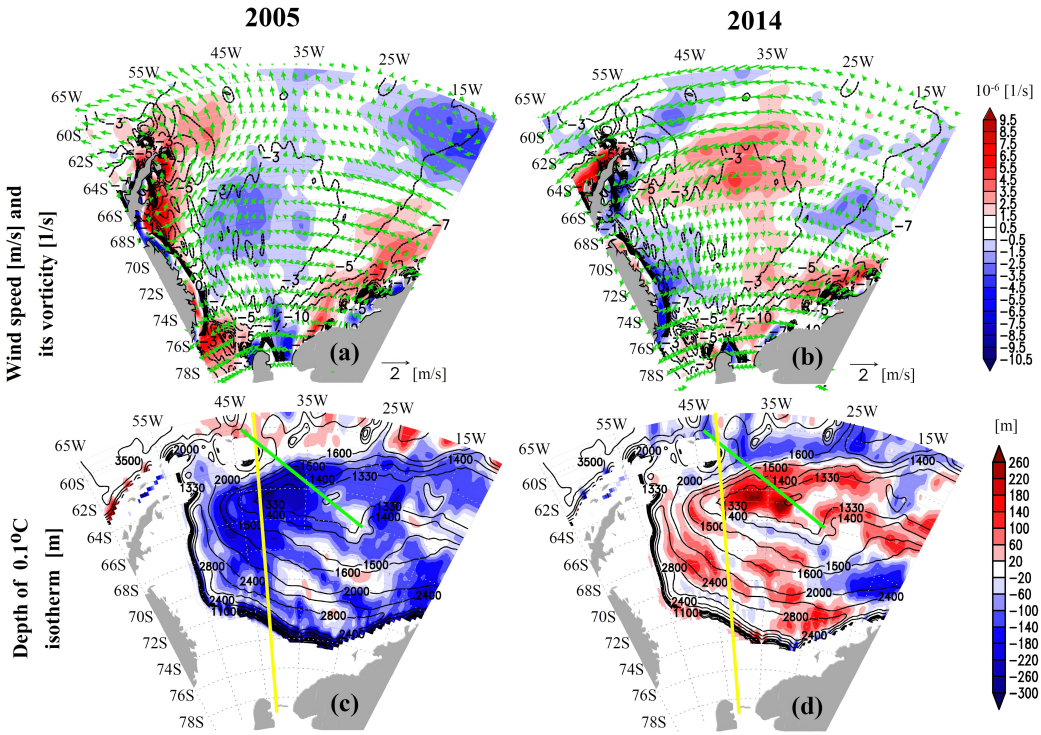

Figure 3. (a) Wind speed mean anomaly by ERA5 datasets (green arrows) (m/s) and its vorticity (shaded) (10^{-6}/s) in 2005, contoured is wind vorticity averaged for 1993–2023 (10^{-6}/s); (b) same as (a), but for 2014; (c) averaged for 1993–2023 depth of isotherm 0.1 °C (contours) and its anomaly (m) in 2005 (shaded); (d) same as (c), but for 2014.

As a result, rise of the Deep Waters in 2005 is stronger than in 2014 (Figure 4b) at the background of the mean for 1993–2023 water rise over almost whole Weddell Sea (Figure 4a).

This more intensive rise of waters in 2005, comparative to 2014, is well pronounced at the sections of potential temperature, density and salinity along 42°W at Figure 5 (the position of the section is shown via yellow line at Figure 4). In 2005, isotherms, isohalines and isopycnals (Figure 5a,c,e)in the area 69–63°S noticeably rise to the surface and deepen near the edges of the section. In 2014, the inverse pattern is observed (Figure 5b,d,f).

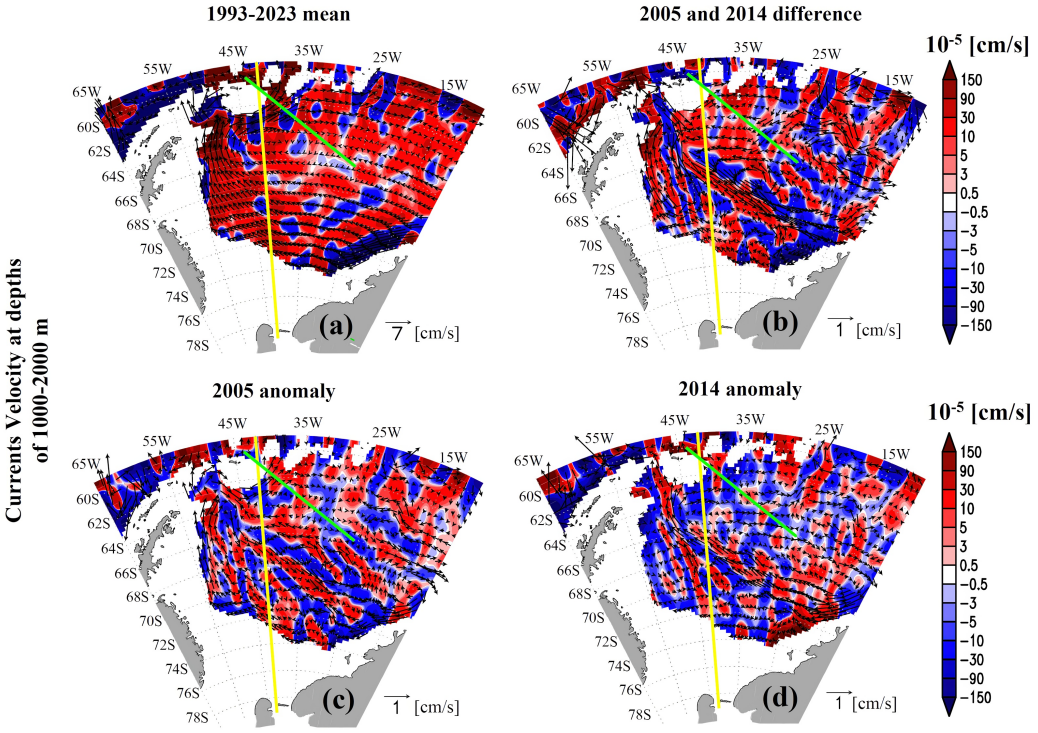

Figure 4. (a) Current velocity in Weddell Sea averaged for 1993–2023 and over depth 1000–2000 m (cm/s) (black arrows) and vertical velocity (10^{-5} cm/s) (shaded); (b) same as (a), but for difference between 2005 and 2014; (c) same as (a), but for anomaly of 2005 relative to period 1993–2023; (d) same as (c), but for 2014. To obtain more homogeneous pattern, all the current velocity components were smoothed (about 15 times) using the 9-point filter from the package OpenGrADS (https://meteocenter.net/weather/grib_data/grads1_9/grads-1.9b4/doc/gradfuncsmth9.html). Yellow and green lines present the sections crossing the Orkney Passage.

The similar structure is observed at the section crossing the Orkney Passage (along the green line from (25.75°W, 66°S) to (43.75°W, 60°S)) presenting the intensive rise of waters in 2005 (black contours) comparative to 2014 (yellow contours), which is well pronounced at the sections of potential temperature, salinity and density (Figure 6). In 2005, black isotherms, isohalines and isopycnals (Figure 6) in the area 65–62°S noticeably rise to the surface, while they deepen and enclose near bottom in the Orkney Passage from 62°S to 60°S. In 2014, the opposite pattern was observed (Figure 6): yellow isotherms, isohalines and isopycnals become flatter in the center of the section, while they turn northward in the Orkney Passage, which is supposed to amplifying deep water recirculation in the passage.

In the previous paper [*Morozov et al.*, 2024], we demonstrate the mechanism of water recirculation in the Orkney Passage based on numerical simulation by using "diagnosis-adjustment" technique [*Sarkisyan and Sündermann*, 2009] with the model INMOM (Institute of Numerical Mathematics Ocean Model) [*Gusev et al.*, 2025] based on the EN4 datasets.

These results are also confirmed by the ORAS5 data. Figure 7g demonstrates that, on average, the waters move from the Weddell Sea to the Scotia Sea for the period 1993–2023 at the depth 2429 m. However, the transport through the Orkney Passage was almost unchanged in 2005 (Figure 7e), while it increased in 2014 (Figure 7f). When the central part of the WSDW dome moves up, (Figure 6 and Figure 5), its peripheral parts move down, and vice versa. The moving up or down in the area of the northern boundary of the Weddell Sea leads to either warmer or colder water overflow through the crest of the South Scotia Ridge. Thus, colder or warmer AABW move into the Scotia Sea and, further, into the Southeast Atlantic. Negative anomalies of temperature and salinity in the Orkney Passage and Scotia Sea in 2014 (Figure 7b,d), comparative to positive ones in 2005 (Figure 7a,c) confirm the process.

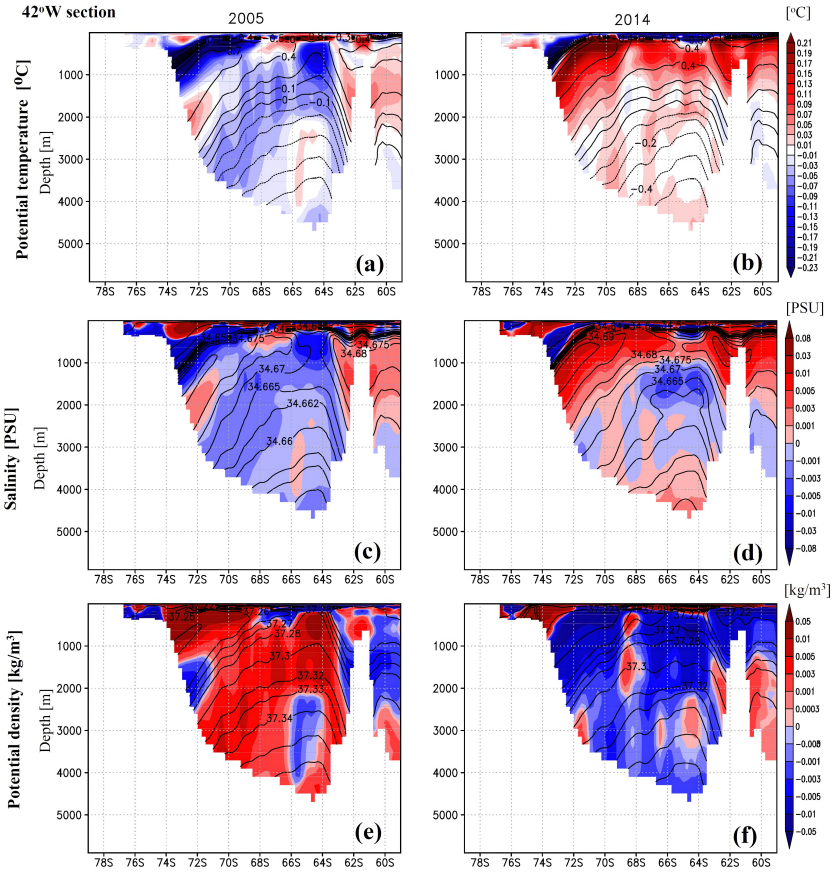

Figure 5. A section along 42°W (yellow line at Figure 4) of potential (at 2000 m depth) temperature °C (contours) for (a) 2005 and (b) 2014, shaded are potential temperature anomalies relative to its mean for 1993–2023; (c) and (d) same as (a) and (b), but for salinity (PSU); (e) and (f) same as (a) and (b), but for potential (at 2000 m depth) density kg/m^3.

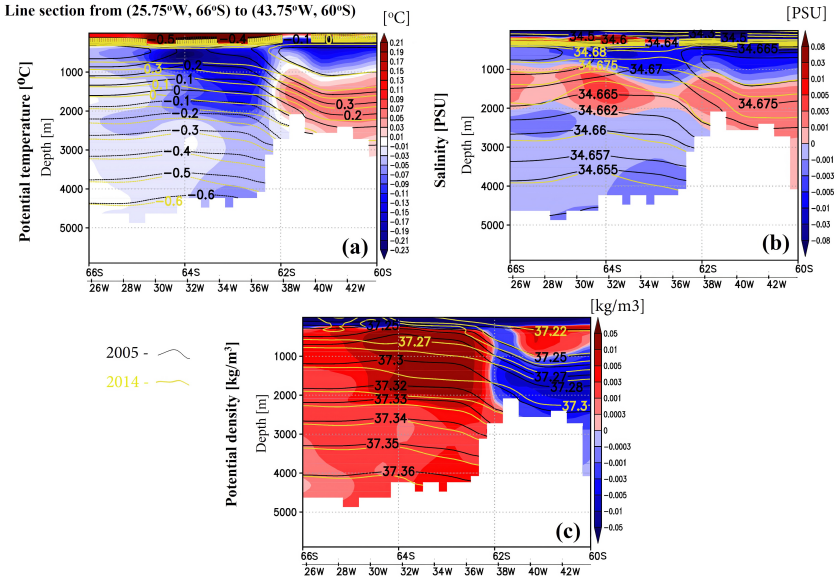

Figure 6. A section along the line (25.75°W, 66°S)–(43.75°W, 60°S) (green line at Figure 4) of (a) potential (at 2000 m depth) temperature °C, (b) salinity (PSU) and (c) potential (at 2000 m depth) density kg/m^3. Black contours present mean for 2005, yellow contours present mean for 2014, shading present their difference.

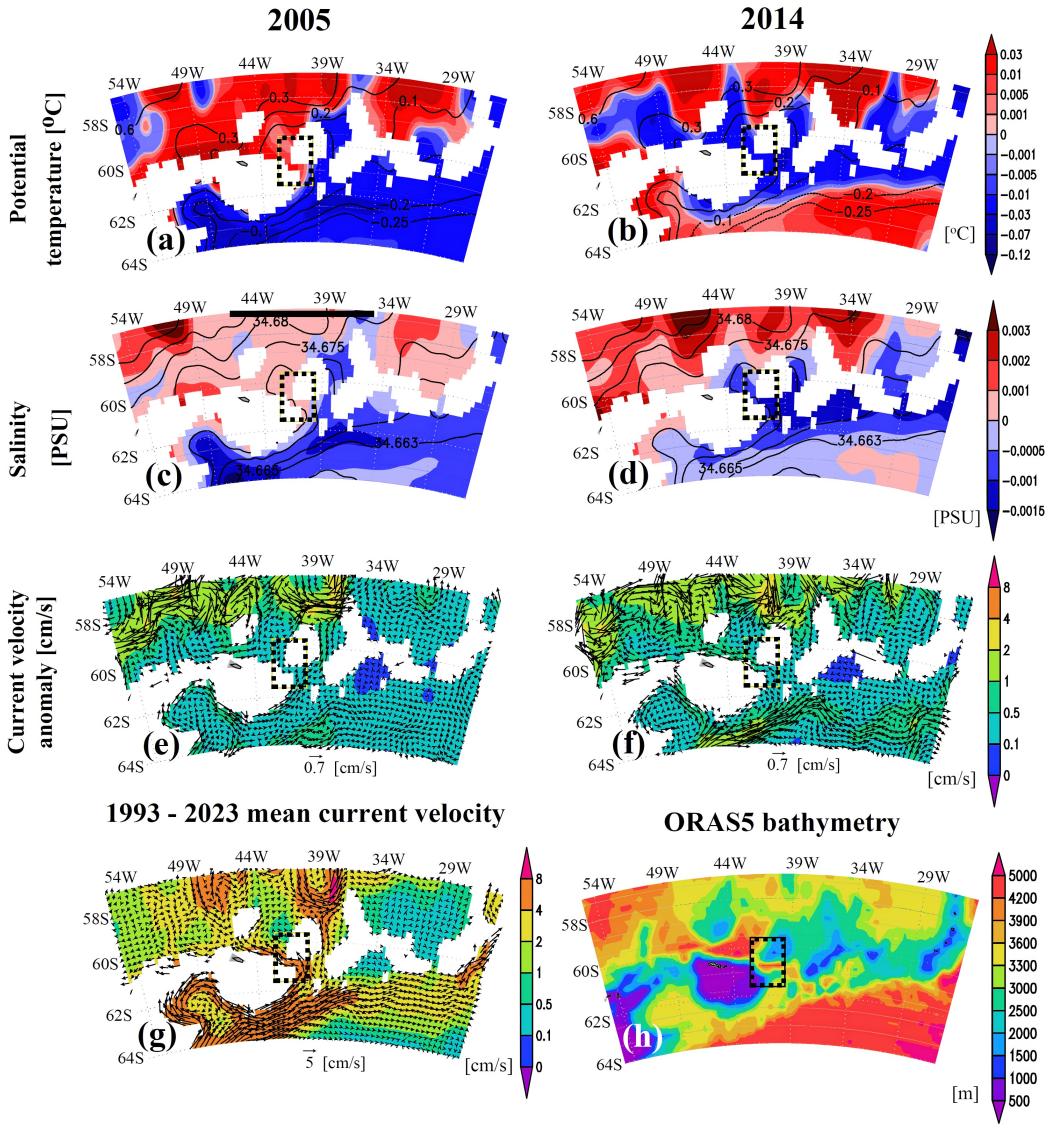

Figure 7. Surrounding of the South Scotia Ridge by the ORAS5 datasets: mean for 1993–2023 (contours) and anomalies relative to this mean (shaded): potential temperature °C in (a) 2005 and (b) 2014; salinity (PSU) in (c) 2005 and (d) 2014; anomalies of current velocity (cm/s) in (e) 2005 and (f) 2014 relative to (g) mean for 1993–2023 at the depth 2429 m, shaded is vector magnitude, the Orkney Passage is marked as a black dotted line; (h) ORAS5 Bathymetry of the seafloor (m) in the vicinity of the South Scotia Ridge.

4. Discussion and Conclusions

Investigation of the cyclonic activity influencing WSDW propagation in high latitudes is of great significance. AABW transport from the Weddell Sea is of variable rate, however, it keeps stable direction of the stream. It was noted in [*Gordon et al.*, 2010] that there is a seasonal cycle of abyssal water temperature with the maximum of the cold layer in May–June and of the warm one in October–November, although exact temporal frames vary annually. The coldest layers were recorded in 1999 and 2002, while the cold period was missing in 2000.

Current velocity and water mass characteristics allow one to suppose that cold and warm streams are originated in the Weddell Sea southeastern area. Seasonal variations of bottom water properties are accounted for with wind fluctuations along the Weddell Sea western boundaries, while interannual evolution is concerned with change in wind cyclonic structure and global climatic factors.

It was demonstrated in [*Abrahamsen et al.*, 2019] that, starting from 2014, one can observe stabilization of AABW volumes in the Scotia Sea, the tendency to decreasing amount of transported waters is terminating, and, respectively, contribution to Atlantic meridional circulation decreases. The greatest decrease in the volume of the AABW densest layers was observed since early 90s up to 2014, after which a partial restoring started, what is shown above.

The north-directed transport of WSDW occurs northward from the Weddell Sea through several gaps in the South Scotia Ridge. Cyclonic circulation in the Weddell Sea results in the dome-shaped structures of isopycnals and isotherms. When the WSDW circulation intensifies, the slope of dome contours become steeper, the isotherms at the periphery of the Weddell Sea descend and only warmer water can overflow the crest of the Orkney Passage over the sill at 3600 m. When wind weakens, the WSDW dome (all isotherms and isopycnals) becomes flatter. The isotherms at the periphery of the sea ascend; therefore, colder water flows through the Orkney Passage. This was suggested in [*Meredith et al.*, 2008] and shown above by using ORAS5 datasets. Due to the observed variations in the overflow of bottom waters, the transformed waters with the variations in the bottom water potential temperature up to ±0.02 °C are observed up to the latitudes of the Vema Channel (34°S) further [*Morozov et al.*, 2021].

Acknowledgments. The study was conducted under the state assignment to the Lomonosov Moscow State University (no. 122052000076-3) in the part of data processing, federal assignment to the Shirshov Institute of Oceanology RAS (no. FMWE-2024-0016) in the part of oceanological investigation, and the Moscow Center of Fundamental and Applied Mathematics at INM RAS (Agreement no. 075-15-2025-347 with the Ministry of Education and Science of the Russian Federation) in the part of numerical analysis of the data. The data presented in this study are available at https://data.marine.copernicus.eu/product/GLOBAL_MULTIYEAR_PHY_ENS_001_031. Data processing was performed with using the equipment of the Center for Collective Use of Ultra-High-Performance Computing Resources of Lomonosov Moscow State University [*Voevodin et al.*, 2019] and the Joint SuperComputer Center of the Russian Academy of Sciences.

References

Abrahamsen E., Meijers A., Polzin K., et al. Stabilization of dense Antarctic water supply to the Atlantic Ocean overturning circulation // Nature Climate Change. — 2019. — Vol. 9, no. 10. — P. 742–746. — https://doi.org/10.1038/s41558-019-0561-2.

Balmaseda M., Hernandez F., Storto A., et al. The Ocean Reanalyses Intercomparison Project (ORA-IP) // Journal of Operational Oceanography. — 2015. — Vol. 8, sup1. — https://doi.org/10.1080/1755876x.2015.1022329.

Bernard B., Madec G., Penduff T., et al. Impact of partial steps and momentum advection schemes in a global ocean circulation model at eddy-permitting resolution // Ocean Dynamics. — 2006. — Vol. 56, no. 5/6. — P. 543–567. — https://doi.org/10.1007/s10236-006-0082-1.

Breivik Ø., Mogensen K., Bidlot J. R., et al. Surface wave effects in the NEMO ocean model: Forced and coupled experiments // Journal of Geophysical Research: Oceans. — 2015. — Vol. 120, no. 4. — P. 2973–2992. — https://doi.org/10.1002/2014jc010565.

Campos E., Caspel M. van, Zenk W., et al. Warming Trend in Antarctic Bottom Water in the Vema Channel in the South Atlantic // Geophysical Research Letters. — 2021. — Vol. 48, no. 19. — https://doi.org/10.1029/2021GL094709.

Coles V., McCartney M., Olson D., et al. Changes in Antarctic Bottom Water properties in the western South Atlantic in the late 1980s // Journal of Geophysical Research: Oceans. — 1996. — Vol. 101, no. C4. — P. 8957–8970. — https://doi.org/10.1029/95jc03721.

Donlon C., Martin M., Stark J., et al. The Operational Sea Surface Temperature and Sea Ice Analysis (OSTIA) system // Remote Sensing of Environment. — 2012. — Vol. 116. — P. 140–158. — https://doi.org/10.1016/j.rse.2010.10.017.

Fichefet T. and Maqueda M. Sensitivity of a global sea ice model to the treatment of ice thermodynamics and dynamics // Journal of Geophysical Research: Oceans. — 1997. — Vol. 102, no. C6. — P. 12609–12646. — https://doi.org/10.1029/97jc00480.

Gordon A., Huber B., McKee D., et al. A seasonal cycle in the export of bottom water from the Weddell Sea // Nature Geoscience. — 2010. — Vol. 3, no. 8. — P. 551–556. — https://doi.org/10.1038/ngeo916.
Gouretski V. and Danilov A. Weddell Gyre: structure of the eastern boundary // Deep Sea Research Part I: Oceanographic Research Papers. — 1993. — Vol. 40, no. 3. — P. 561–582. — https://doi.org/10.1016/0967-0637(93)90146-t.
Gouretski V. and Reseghetti F. On depth and temperature biases in bathythermograph data: Development of a new correction scheme based on analysis of a global ocean database // Deep Sea Research Part I: Oceanographic Research Papers. — 2010. — Vol. 57, no. 6. — P. 812–833. — https://doi.org/10.1016/j.dsr.2010.03.011.
Gusev A., Diansky N., Fomin V., et al. The Model of Oceanic and Marine Circulation INMOM: From Origins to the Present Day // Izvestiya, Atmospheric and Oceanic Physics. — 2025. — Vol. 61, no. 3. — P. 311–324. — https://doi.org/10.1134/s0001433825700653.
Keeley S. and Mogensen K. Dynamic sea ice in the IFS // ECMWF Newsletter. — 2018. — P. 23–29. — https://doi.org/10.21957/4SKA25FURB.
Keeley S., Mogensen K., Bidlot J. R., et al. Introduction of a new ocean and sea-ice model based on NEMO4-SI3 // ECMWF Newsletter. — 2024. — P. 24–29. — https://doi.org/10.21957/SK4928DS0A.
Madec G. and the NEMO team. NEMO Ocean Engine. Version 3.6 stable. — 2008. — URL: https://www.nemo-ocean.eu/doc/.
McDougall T. J. and Barker P. M. Getting started with TEOS-10 and the Gibbs Seawater (GSW) oceanographic toolbox. Version 3.06.12. — SCOR/IAPSO WG127, 2011. — 34 p.
Meredith M., Naveira Garabato A., Gordon A., et al. Evolution of the Deep and Bottom Waters of the Scotia Sea, Southern Ocean, during 1995-2005 // Journal of Climate. — 2008. — Vol. 21, no. 13. — P. 3327–3343. — https://doi.org/10.1175/2007JCLI2238.1.
Morozov E., Bagatinskaya V., Bagatinsky V., et al. Variability of the Temperature Dome of Weddell Sea Deep Water Depending on the Intensity of the Cyclonic Wind Field // Izvestiya, Atmospheric and Oceanic Physics. — 2024. — Vol. 60, no. 5. — P. 579–595. — https://doi.org/10.1134/s0001433824700476.
Morozov E., Frey D., Zuev O., et al. Hydraulically Controlled Bottom Flow in the Orkney Passage // Water. — 2022. — Vol. 14, no. 19. — P. 3088. — https://doi.org/10.3390/w14193088.
Morozov E., Tarakanov R. and Frey D. Bottom Gravity Currents and Overflows in Deep Channels of the Atlantic Ocean: Observations, Analysis, and Modeling. — Cham : Springer International Publishing, 2021. — https://doi.org/10.1007/978-3-030-83074-8.
Naveira Garabato A., McDonagh E., Stevens D., et al. On the export of Antarctic Bottom Water from the Weddell Sea // Deep Sea Research Part II: Topical Studies in Oceanography. — 2002. — Vol. 49, no. 21. — P. 4715–4742. — https://doi.org/10.1016/s0967-0645(02)00156-x.
Penduff T., Juza M., Brodeau L., et al. Impact of global ocean model resolution on sea-level variability with emphasis on interannual time scales // Ocean Science. — 2010. — Vol. 6, no. 1. — P. 269–284. — https://doi.org/10.5194/os-6-269-2010.
Pujol M. I., Faugére Y., Taburet G., et al. DUACS DT2014: the new multi-mission altimeter data set reprocessed over 20 years // Ocean Science. — 2016. — Vol. 12, no. 5. — P. 1067–1090. — https://doi.org/10.5194/os-12-1067-2016.
Reynolds R., Smith T., Liu C., et al. Daily High-Resolution-Blended Analyses for Sea Surface Temperature // Journal of Climate. — 2007. — Vol. 20, no. 22. — P. 5473–5496. — https://doi.org/10.1175/2007jcli1824.1.
Sarkisyan A. and Sündermann J. Nonlinear Models for Diagnostic, Prognostic and Adjustment Calculations of Ocean Climate Characteristics // Modelling Ocean Climate Variability. — Dordrecht : Springer Netherlands, 2009. — P. 67–102. — https://doi.org/10.1007/978-1-4020-9208-4_3.
Voevodin V., Antonov A., Nikitenko D., et al. Supercomputer Lomonosov-2: Large Scale, Deep Monitoring and Fine Analytics for the User Community // Supercomputing Frontiers and Innovations. — 2019. — Vol. 6. — P. 4–11. — https://doi.org/10.14529/jsfi190201.
Zuo H., Balmaseda M., Tietsche S., et al. The ECMWF operational ensemble reanalysis-analysis system for ocean and sea ice: a description of the system and assessment // Ocean Science. — 2019. — Vol. 15, no. 3. — P. 779–808. — https://doi.org/10.5194/os-15-779-2019.